AD-A060 396 ROCKWELL INTERNATIONAL THOUSAND OAKS CALIF SCIENCE --ETC F/G 8/7
EVALUATION OF THE AC AND DC CHARACTERISTICS OF ROCK CONDUCTIVIT--ETC(U)
SEP 78 R M HOUSLEY, J R OLIVER N00014-76-C-0653
UNCLASSIFIED SC5061.1FR NL

1 OF 1
AD
A060396

END
DATE
FILMED
1-79
DDC

12

LEVEL II

SC5061.1FR September 27, 1978

EVALUATION OF THE AC AND DC CHARACTERISTICS OF ROCK CONDUCTIVITY

for period
February 1, 1976 - July 31, 1978

General Order No. 5061

Contract No. N00014-76-C-0653

Prepared for:

Office of Naval Research
Arlington, Virginia 22217

R. M. Housley
Principal Investigator
Science Center, Rockwell International

This work was sponsored by the Office of Naval Research. Reproduction in whole or in part is permitted for any purpose of the United States Government.

Rockwell International
Science Center

UNCLASSIFIED

SECURITY CLASSIFICATION OF THIS PAGE (When Data Entered)

REPORT DOCUMENTATION PAGE	READ INSTRUCTIONS BEFORE COMPLETING FORM
1. REPORT NUMBER (6)	2. GOVT ACCESSION NO. (7) / 3. RECIPIENT'S CATALOG NUMBER (31)
4. TITLE (and Subtitle) (10) EVALUATION OF THE AC AND DC CHARACTERISTICS OF ROCK CONDUCTIVITY,	5. TYPE OF REPORT & PERIOD COVERED (1) Final Report. Feb. 1, 1976 - July 31, 1978
	6. PERFORMING ORG. REPORT NUMBER (14) SC5061.1FR
7. AUTHOR(s) R. M. Housley, Principal Investigator; J. R. Oliver	8. CONTRACT OR GRANT NUMBER(s) (15) N00014-76-C-0653
9. PERFORMING ORGANIZATION NAME AND ADDRESS Rockwell International/Science Center 1049 Camino Dos Rios Thousand Oaks, Ca. 91360	10. PROGRAM ELEMENT, PROJECT, TASK AREA & WORK UNIT NUMBERS None
11. CONTROLLING OFFICE NAME AND ADDRESS (11) Office of Naval Research Arlington, Virginia 22217	12. REPORT DATE September 27, 1978
	13. NUMBER OF PAGES 59
14. MONITORING AGENCY NAME & ADDRESS (if different from Controlling Office) (12) 62p.	15. SECURITY CLASS. (of this report) Unclassified
	15a. DECLASSIFICATION/DOWNGRADING SCHEDULE

16. DISTRIBUTION STATEMENT (of this Report)

Reproduction in whole or in part is permitted for any purpose of the United States Government.

17. DISTRIBUTION STATEMENT (of the abstract entered in Block 20, if different from Report)

18. SUPPLEMENTARY NOTES

19. KEY WORDS (Continue on reverse side if necessary and identify by block number)

waveguide, buffered atmosphere, dielectric constant, conductivity, hydration, granite, mafic rocks.

20. ABSTRACT (Continue on reverse side if necessary and identify by block number)

Results are presented on the AC and DC characteristics of Wausau granite which show that excess AC losses at low temperatures are associated with cracks sealed by rutile, and are independent of any new open cracks. Data is also presented on the effect of surface hydration and contamination in old weatered cracks.

Pyroxene was found to be the apparent major conducting phase in Mellen gabbro using a new scanning electron microscope technique.

DD FORM 1 JAN 73 1473 EDITION OF 1 NOV 65 IS OBSOLETE

UNCLASSIFIED

SECURITY CLASSIFICATION OF THIS PAGE (When Data Entered)

LB

389 949

DD 10 12 035

Rockwell International
Science Center
SC5061.1FR

EVALUATION OF THE AC AND DC CHARACTERISTICS OF ROCK CONDUCTIVITY

R. M. Housley and J. R. Oliver
Science Center, Rockwell International
Thousand Oaks, California 91360

ABSTRACT

Results are presented for Wausau granite which show that the excess AC conduction losses which appear below 500°K for properly cleaned and annealed rocks are associated with rutile sealing cracks, and are independent of any new cracks generated by exposure to high temperatures. Data are also shown on the effect of altered and contaminated surfaces in old cracks, as well as the effect of short term exposure of the rock to water.

The detailed identification of the nature and origin of conduction mechanisms in rocks has been explored using a new scanning electron microscope technique. Preliminary data on Mellen gabbro show that an interconnected network of pyroxenes is largely responsible for the high conductivity observed in this rock. Comparative conductivity results for Skrainka diabase suggest that this may be a general property of deep-seated mafic rocks. Suggested areas for further investigation of the electrical properties of rocks are also presented.

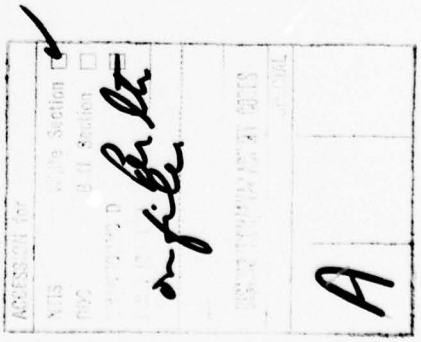

1. Introduction

In our previous report (AGU Monograph 20)[1] we presented data on Montello and Wausau granites which showed large AC conductivities in excess of those at DC for temperatures below 500°K. Since these losses are of interest from both a geophysical and crustal waveguide communication standpoint, we have continued our studies with a series of experiments designed to permit a better understanding of the origin of these losses. In particular, we have explored the functional dependence of the AC losses on microcrack density, as well as on surface contamination and hydration, the results of which will be given here.

It is the general nature of electrical measurements on rocks that such measurements give an average of the various conduction and dielectric loss mechanisms present in the rock as a whole. The association of various electrical phenomena with particular conduction and loss mechanisms is necessarily limited by the averaging nature of the measurement. Although a great deal of information can be obtained through careful experimental design and technique, we wished to explore supplementary techniques which would permit more precise identification of the nature and origin of these mechanisms. To this end we have explored a new experimental technique using a scanning electron microscope as an electrical probe of the various conduction paths present in rocks. In particular, we shall present preliminary results on Mellen gabbro which indicate the dominant conduction mechanism for this high conductivity rock, and possibly deep-seated mafic rocks in general.

2. Samples

Our studies of the conductivity of granite were performed with Wausau granite samples, MIT identification number 1336, supplied to us by Gene Simmons. The use of this rock in the experiments described here permitted a direct comparison with previous data we have collected, as well as a further confirmation of the consistency of results from one sample to the next.

Our sample preparation procedure was essentially the same as described previously [Housley and Oliver, 1977].[1] Briefly, slabs of 2-3 mm thickness were cut from the rock with an oil-water emulsion lubricated diamond saw. The surfaces were then polished with water lubricated 600-grit silicon carbide lapping paper, and then repeatedly rinsed in acetone. The samples were then given an ultrasonic cleaning in distilled water, and then a final rinse in distilled water prior to drying.

The electrical contacts were formed by sputtering platinum onto the sample surface with the use of appropriate masks. Although we have formed contacts in the past using a colloidal platinum suspension, the sputtered contacts were deemed preferable since they did not require low temperature heating prior to any electrical measurements. These contacts were found to be very stable, and did not exhibit any tendency to lift during the course of the experiments.

3. Electrical Measurement

Our measurements were performed using a guarded three-terminal configuration [Morin, et al., 1977].(2) The DC conductivity measurements were made using a Keithley 610-C electrometer as a virtual-ground current amplifier. Because of a desire to minimize any contact polarization effects, particularly at high temperatures, which might arise from the use of a constant DC potential across the sample, a low frequency (1.10 Hz) sine-wave voltage was applied to the high side of the sample. The sample current was detected by phase-locked amplification of the electrometer output using a PAR 124 lock-in amplifier. Hence, our "DC" results are not true DC, but rather a low frequency approximation. The use of a low frequency technique has the additional advantage of permitting the observation on an oscilloscope of any signal distortion due to poor electrical contacts as well as being more compatible with low frequency geophysical field measurements.

The AC conductance and capacitance measurements were performed with either a General Radio 1615A capacitance bridge or a Hewlett-Packard 4270A automatic bridge, again using a standard three-terminal configuration. Both AC and low frequency "DC" measurements were made with low voltages, typically on the order of 1-10 volts/cm. The measured sample conductance and capacitance were virtually insensitive to the applied voltage in all of the experiments to be described here, indicating good ohmic contact behavior.

4. Experimental Results

4.1 Granite

Studies by Simmons and Cooper (1977) on Westerly granite indicate that a substantial increase in crack porosity can be expected for granites heated above 500°K.[3] Since our own results on the electrical properties of Montello and Wausau granites showed AC conductivities well above the DC results for temperatures below 700°K, we wished to explore the possibility that these excess AC losses might have some functional dependence on the density of microcracks in the rock. To this end we selected a Wausau granite sample which had no prior heat treatment, and continuously monitored its AC conductivity at 10 kHz as the sample was cycled to progressively higher temperatures.

A complicating factor in such a series of experiments is the fact that the low temperature conductivity of a rock with no previous thermal history is dominated by the conductivity due to carbonaceous material initially in the cracks. Such material may occur either naturally or as a result of sample preparation procedures. Our previous work on granite has shown that the presence of such carbonaceous material leads to excess conductivities which are largely irreproducible with successive thermal cycling. Therefore, it is essential that this material be removed at the lowest possible temperatures prior to any high temperature annealing. Since a dry oxygen atmosphere has proven to be most effective in the removal of this material, while at the same time providing low overall rock conductivities, this atmosphere was used in our intial warming experiments.

The 10 kHz AC conductivity of Wausau granite 1336-2 for several thermal cycles is shown in Fig. 1. The initial warming curve A shows the effect of carbonaceous material and surface alteration in the cracks. Such a high excess conductivity is typical of the AC and DC conductivities of granite on initial warming, but it is by no means unique, nor does it in any way represent an equilibrium condition, since a slow decrease in conductivity can be observed at any constant temperature above ~ 150°C. As a result, such initial warming curves tend to be quite ragged and irreproducible.

A sequence of slow cooling runs were then taken after 1-2 hour annealing at successively higher temperatures, samples of which are shown in curves B, C and D of Fig. 1. Cooling was commenced after no significant change in conductivity could be observed at a particular soak temperature over a 30-minute period. The most dramatic decrease in conductivity took place during the initial soak at 540°K, as seen from curve B. No significant change in the low temperature conductivity was observed for soak temperatures above 700°K, although the high temperature AC conductivity, which is asymptotic to the DC curve, continued to show small decreases up to 830°K. Long term ($>$30 hours) annealing at or above this temperature showed no further change in conductivity.

The observed change in conductivity during the course of these experiments was in all cases monotonically decreasing. The final equilibrium conductivities, both AC and DC, were in excellent agreement with previous measurements we have made on this rock in an oxidizing atmosphere, as well as being similar to those for other granites.[1] In an earlier

series of experiments we had observed a minimum AC loss a factor of 3-5 below the minimum values obtained in the present experiments. This minimum was observed at 520°K after partial reduction in a dry N_2 atmosphere with a subsequent reoxidation. However, the sample was still in an altered condition at this point, and in fact the DC conductivity did not achieve a minimum value until the sample had been subsequently cycled to 780°K in oxygen, whereupon the AC losses rose to their equilibrium values, and remained there independent of any further high temperature cycling. In the present series of experiments we observed only a monotonic decrease of the AC losses down to their steady state values. The discrepancy in behavior for the two series of experiments is difficult to understand; however, the minimum AC losses observed earlier clearly did not represent an equilibrium condition for the rock, and it is likely that different samples may display different conductivity behavior until surface contamination, alteration and damage have been minimized. The excellent agreement and reproducibility of conductivity data for different samples which have been properly cleaned and equilibrated leads us to the conclusion that only such data is truly representative of the rock.

The AC and DC conductivity for Wausau granite 1336-2 in oxygen are shown as the dashed lines in Fig. 2. The results of our experiments indicate that the excess AC losses are not associated with the presence of new cracks generated by cycling to elevated temperatures; the same conclusion applies to the DC conductivity as well. Conductivity data for the same sample in a magnetite-hematite buffered N_2 atmosphere are shown as the solid lines in Fig. 2. Mössbauer data on the Wausau granite indicate the

magnetite buffered N_2 atmosphere comes close to simulating the environment in which the rock last equilibrated, and therefore is more representative of the rock conductivity in situ. The data of Fig. 2 clearly show higher overall conductivities for the more reducing buffered N_2 atmosphere as compared to the data for oxygen, although at DC the difference is relatively small. The observed changes in conductivity were completely reversible with re-oxidation of the sample. The similarity of the data presented in Fig. 2 reflects the general observation that the conductivity of granite is relatively insensitive to partial oxygen pressure for all except highly reducing H_2-N_2 environments.

Data for the relative dielectric constant, ε' of Wausau granite in the magnetite buffered N_2 atmosphere are shown as a function of frequency in Fig. 3. The high temperature excess dielectric constant is approximately a factor of 2 lower than that in oxygen, but otherwise is similar in form to previous granite data for an oxidizing environment. The rise in dielectric constant begins to occur at the point in temperature and frequency where the DC conduction current becomes comparable to the dielectric displacement current, and therefore is not associated with the excess AC conduction losses which appear at lower temperatures. The excess dielectric constant may be due to interfacial polarization associated with conduction through the major mineral phases, or with charge build-up along grain boundaries and cracks. Another possibility is contact polarization. Such polarization may occur even for contacts which display ohmic or non-blocking behavior,[4] evidenced here by the asymptotic behavior of the conductivity curves at high temperatures (Fig. 2) and the lack of any

observable distortion in the current waveform. The data accumulated at present is inconclusive with regard to which polarization mechanism is dominant. However, the observed excess dielectric constant remains of minor geophysical importance since it occurs only at temperatures in excess of those expected in the upper crust.

All of the data presented is representative of granite conductivity in a dry environment. Since the presence of contaminated or altered crack surfaces can have a substantial influence on the electrical behavior of the rock, we performed some initial conductivity experiments in a wet atmosphere to see how water would affect these surfaces. Representative conductivity data for a previously equilibrated Wausau granite sample in wet oxygen are shown in Fig. 4, along with comparative data for the same sample in a dry oxygen atmosphere. The wet oxygen atmosphere was obtained by bubbling oxygen gas through de-ionized water at 24°C prior to its introduction into the furnace tube.

It can be seen in Fig. 4 that the presence of water affects granite conductivity only below 130°C. Below 50°C the conductivity is dominated by the DC value and is essentially independent of frequency. In general, the presence of water on exposed surfaces has a substantial influence on the DC or low frequency conductivity at low temperatures, but does not appear to change the excess high frequency losses to any great extent. Since the AC losses are not associated with the density of new microcracks generated by high temperature annealing, it appears then that these losses must be associated in some way with the presence of sealed microcracks in

the rock. However, high AC losses are observed for rocks which have a significant amount of surface contamination and alteration, as discussed earlier. Hence, these losses may be associated with old open microcracks as well. The fact that there was no observable influence of water on the excess AC conductivity arising from old open cracks might be explained by the weak conditions of surface hydration in these experiments. The degree of surface alteration due to the hydration of Fe-bearing minerals under these conditions is expected to be small compared to the long-term exposure of the rock to ground water, the effect being limited to perhaps only the first one or two monolayers. The fact that the rock conductivities reverted to their previous values with exposure to a dry atmosphere tends to support this viewpoint.

The high value of DC conductivity between 50-130°C in wet oxygen is also interesting since there is less than a monolayer of surface coverage by water in this region. Clearly, more work needs to be done in understanding the effect of water on the AC and DC conductivity of granite before any firm conclusions can be drawn.

4.2 Skrainka Diabase

Because as previously reported (AGU monograph 20) the electrical conductivity of Mellon gabbro is surprisingly high, we decided to measure another deep-seated mafic rock to see if such rocks show high conductivities in general. We chose a sample of Skrainka diabase, MIT number 1415, and painted 1 inch diameter electrodes on opposite faces separated by 1¼ inch, using colloidal graphite suspended in propanol. We then heated the sample to 200°C in a drying oven and measured the resistance between the electrodes

with an ohmmeter. Results were very similar to those obtained in the same way on Mellon gabbro, which in turn agree with those obtained on a smaller sample in the conventional manner. Therefore, we conclude that Skrainka diabase has electrical properties similar to those we reported for Mellon gabbro.

5. Scanning Electron Microscope Studies

During the past several months we have started developing new scanning electron microscope techniques aimed at allowing us to identify the high electrical conductivity paths through rocks. The initial results are very exciting. Not only can the original goal be easily achieved, but the technique can also be used to quickly map mineralogies and provide detailed petrographic descriptions of the samples.

The essential features of the apparatus are schematically illustrated in Fig. 5. The sample is in the form of a polished slab about 1 mm thick, with a clean uncoated front surface and an electrical contact on the back. It is supported on an insulated holder and connected to an electrical feed-through. This in turn is connected to ground either directly or through an electrometer. The focusing conditions in the electron column are nominally chosen so that the beam current, I, incident on the sample is about 4×10^{-10} amp.

Assuming a sample dielectric constant of about 10, if no secondary electrons escaped from the sample and no current flowed through it, the surface potential, V, would increase at the rate of

$$\frac{V}{t} = \frac{I}{C} \quad \frac{5 \times 10^3}{A\ (mm)^2} \quad \text{volt/sec}$$

where C is the capacitance which in turn depends on A, the area being scanned. The sample could thus rapidly charge up to high voltage and deflect the beam.

Taking into account conductivity but still neglecting secondary electron emission, the sample would charge to an equilibrium potential given by

$$V = \frac{\rho \ell I}{A}$$

where ρ is the resistivity and ℓ is the thickness. For example, if $A = 1\ mm^2$, then V = 1000 volts for $\rho = 2.5 \times 10^{11}$ ohm-cm. In the actual experiments material much less resistive than this appears conducting and material much more resistive appears insulating. The secondary electron yield of insulating materials is generally greater than one for incident beam energies roughly in the range from 1 to 3 keV. For higher incident beam energies it falls to lower values.

Data from one of our exploratory runs on a Mellon gabbro sample are presented in Fig. 6. We started with a beam voltage of 2.5 keV. The electrometer showed a positive current flow indicating a secondary electron yield greater than one everywhere on the sample. Only small positive potentials build up on the surface and the image is essentially undistorted under these conditions. The brightness increases directly with conductivity. In the small region shown in Fig. 6a. iron-titanium oxides are bright while pyroxenes are a dull grey and feldspars are black.

When the incident beam energy is increased to 5 keV, the secondary electron yield is near one and the contrast in the image becomes small. Small positive and negative currents are observed when the beam is scanned over the sample. This situation is illustrated in Fig. 6b.

Increasing the beam energy to 10 keV results in negative currents indicative of secondary electron yields less than one over the whole sample. Under these conditions large negative potentials can exist on the sample surface and the image becomes distorted. The contrast also reverses, with insulating regions becoming bright and conducting regions becoming dark. This situation is shown in Fig. 6c. The feldspars are bright, but distorted. The pyroxenes as well as the oxides are dark, indicating their resistivities are of the same order as those observed in bulk Mellon gabbro. Fig. 6d at lower magification and 2.5 keV shows that some cracks and grain boundaries as well as the oxides are highly conducting.

It seems apparent from these exploratory results that this technique has tremendous potential as a method of studying the mineralogy and electrical properties of rocks.

6. Discussion

In our previous report we explicitly discussed the possible influence of cracks on the measured electrical properties of dry rocks. All natural cracks that existed while the rocks were in the ground have been exposed to ground water for a long period of time. This invariably will have produced some leaching and hydration of susceptible mineral surfaces.

In addition to open cracks, the Wausau granite also contains a network of reddish colored sealed cracks in the feldspar, as well as disseminated dark grains. Scanning electron microscope examination shows that the dominant mineral sealing the cracks is rutile. Mössbauer studies show that a major fraction of the iron in the samples is in the form of hematite which might also contribute to the observed red color. Hematite exposed in the cracks would be expected to partly hydrate to FeOOH while sodium, potassium, and calcium would be leached out of the feldspar. Irreversible changes in electrical properties of these samples during the first heating cycle can probably be ascribed to reoxidation of hydrated surfaces as well as the removal of carbonaceous residues.

Since no attempt has been made to replace the missing cations, surfaces affected by leaching are not restored to their original state. Hopefully, however, the aluminum silicates resulting from dehydration will have low electrical losses.

It is well known that the electrical properties of rutile are a sensitive function of its oxidation state and the same may be true for other minerals. The presence of abundant hematite in Wausau granite

indicates that it last equilibrated with oxygen partial pressures at least as high as the magnetite-hematite buffer. Therefore, all our measurements have been made either using this buffer or in a more oxidyzing atmosphere. The higher values of AC losses in the buffered atmosphere support the idea that these losses are largely associated with rutile sealing cracks in the rock.

The initial SEM results on Mellen gabbro tend to show that the previously reported high conductivity for this rock is due to an interconnected network of anomalously conducting pyroxene. Although the gabbro also contains regions of high conductivity due to iron-titanium oxides, these oxides do not appear to form interconnected paths through the rock, and therefore should not substantially influence the DC conductivity.

7. Summary

We have presented results for Wausau granite which show that the excess AC conductivity losses are associated with rutile sealing cracks in the rock. These losses are a function of the oxidation state of rutile, increasing with decreasing partial oxygen pressure. Additional excess AC and DC conductivities due to carbonaceous residues and the hydration of old open cracks were also observed, with irreversable reductions in conductivity upon exposure of the rock to a dry oxygen atmosphere at moderate temperatures. Neither AC or DC conductivity showed any dependence on the density of new microcracks generated by high temperature annealing.

We have explored a new scanning electron microscope technique which permits the identification of high conductivity paths in rocks. Experiments on Mellen gabbro indicate that the previously reported high conductivity of this rock is due to an interconnected network of pyroxenes. The similarity of the mineralogy and conductivity of Skrainka diabase to Mellen gabbro suggests the likelihood that this observation applies to deep-seated mafic rocks in general.

Finally, we have continued our analysis of extensive electrical measurements on forsterite, Mg_2SiO_4, with the objective of clearly defining their geophysical consequences. This work is described in a manuscript attached as Appendix 1.

8. Acknowledgements

We gratefully acknowledge the comments and suggestions made by Gene Simmons and John G. Heacock during the course of this work. We are especially grateful to Gene Simmons for the collection of carefully selected and well-documented samples he has supplied to us for these experiments.

The measurements discussed here and the preparation of this manuscript were supported by Contract N00014-76-C-0653 with the Office of Naval Research. Our work on forsterite was also partially supported by this contract.

REFERENCES

1. R. M. Housley and J. R. Oliver, "Electrical Characteristics of Igneous Precambrian Basement Rocks of Central North America", American Geophysical Union Monograph 20 (1977), 181.

2. F. J. Morin, J. R. Oliver and R. M. Housley, "Electrical Properties of Forsterite, Mg_2SiO_4", Physical Review B. 16(10) (1977), 4434.

3. G. Simmons and H. W. Cooper, "Thermal Cycling Cracks in Three Igneous Rocks", to be published.

4. F. J. Morin, J. R. Oliver and R. M. Housley, "Electrical Properties of Forsterite, Mg_2SiO_4 (III)", to be published.

FIGURE CAPTIONS

Fig. 1 The 10 kHz conductivity of Wausau granite 1336 in oxygen as a function of reciprocal temperature for a sample with no prior thermal history. Curve A is the initial warming of the sample. Curves B, C, and D are slow cooling runs after 1-2 hour soaks at the indicated temperatures. Curve D is very close to the final steady state conductivity for this rock.

Fig. 2 The AC and DC conductivity of Wausau granite after proper cleaning and equilibration. The solid lines are data for a magnetite-hematite buffered N_2 atmosphere, and the dashed lines are those for un-buffered O_2.

Fig. 3 The relative dielectric constant, ε', as a function of reciprocal temperature for Wausau granite in a magnetite buffered N_2 atmosphere. These data are similar to, but somewhat lower than, those for O_2 at high temperatures.

Fig. 4 The 10 kHz and 1.10 Hz "DC" conductivity of Wausau granite in a wet and dry oxygen environment. Note that there is no major influence of water above 150°C.

Fig. 5 Schematic illustration of experimental arrangement used during SEM studies of rock conductivity. Front surface of sample is uncoated. Back surface has a thick sputtered gold coating for electrical contact.

Figure Captions (Continued)

Fig. 6 SEM photographs of uncoated Mellon Gabbro sample at various beam voltages.

a) At 2.5 keV highly conducting Fe, Ti, oxides are bright.

b) At 5.0 keV oxides are brighter but contrast is much lower.

c) At 10.0 keV oxides are black and non-conducting feldspars are bright.

d) Larger area scan at 2.5 keV shows cracks and some grain boundaries are also conducting.

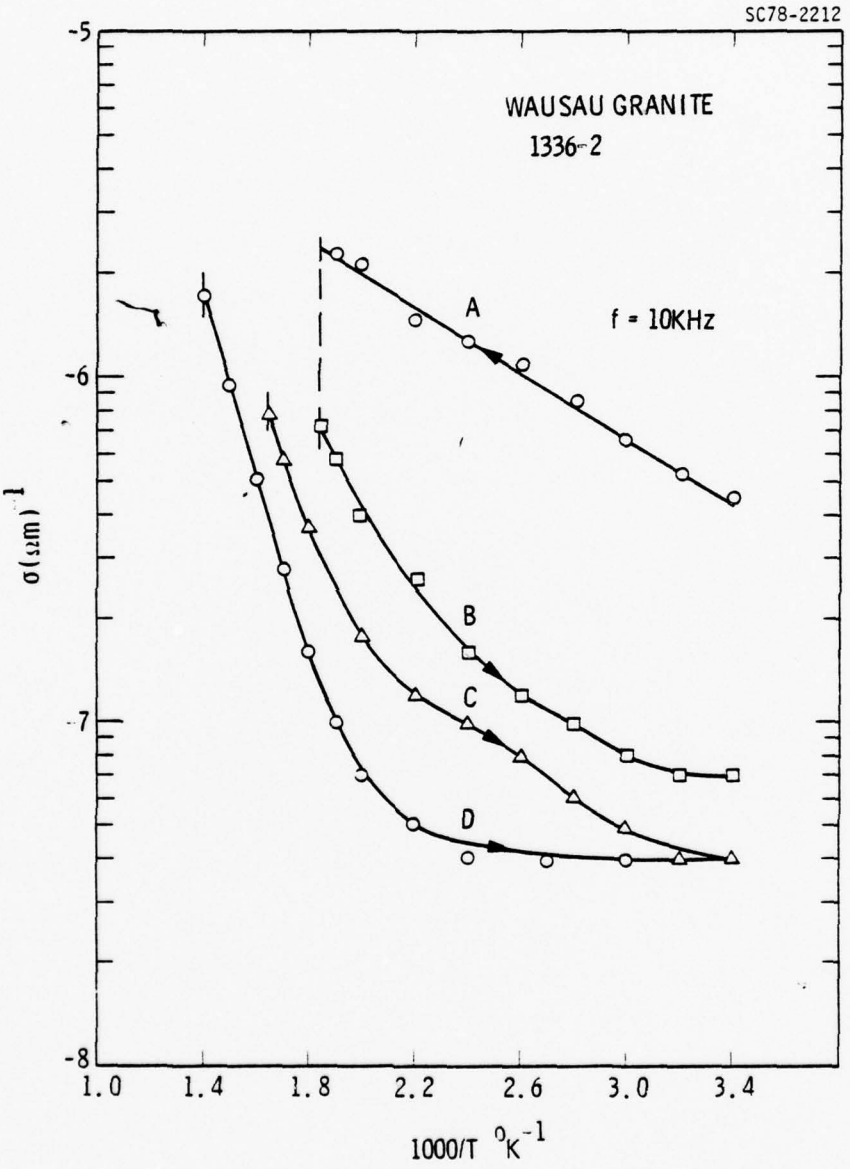
SC78-2212
WAUSAU GRANITE
1336-2
f = 10KHz
A
B
C
D
-5
-6
-7
-8
σ(Ωm)⁻¹
1.0
1.4
1.8
2.2
2.6
3.0
3.4
1000/T °K⁻¹

Fig. 1

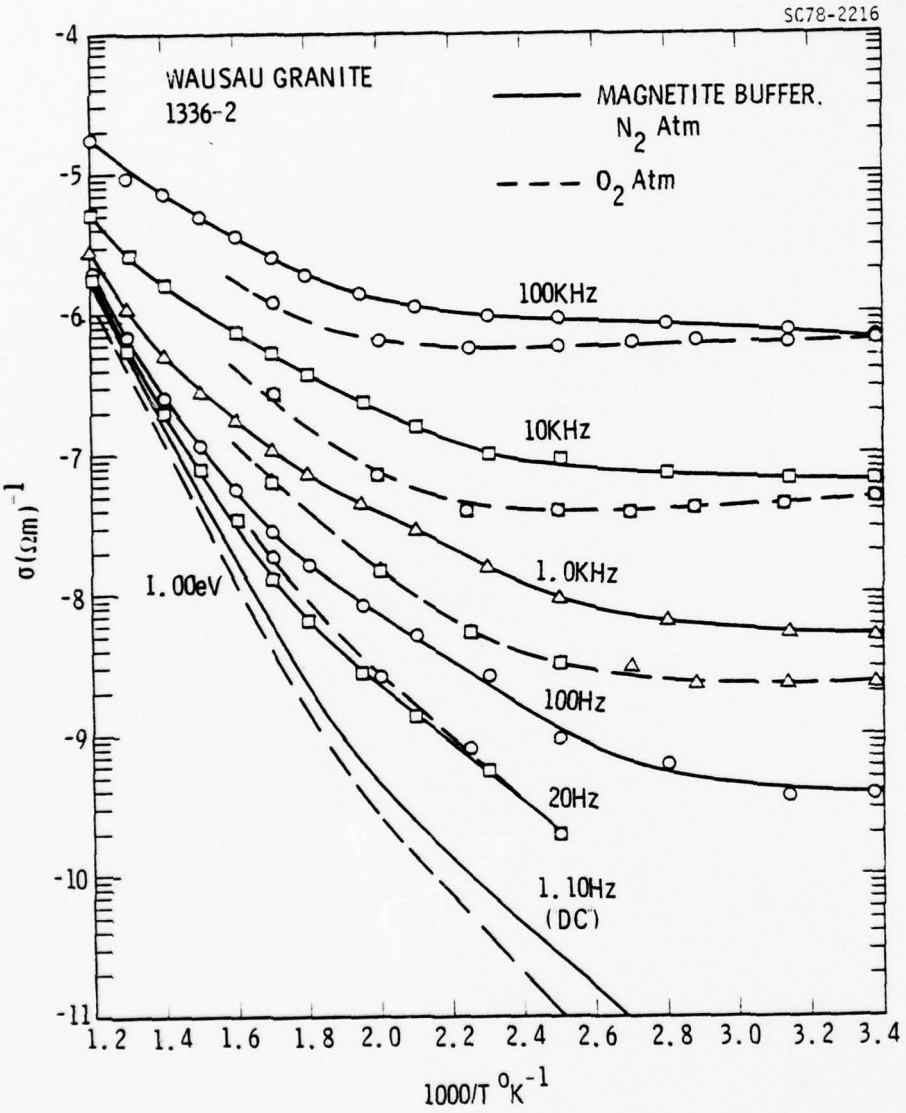
SC78-2216
WAUSAU GRANITE
1336-2
MAGNETITE BUFFER.
N_2 Atm
O_2 Atm
100KHz
10KHz
1.0KHz
100Hz
20Hz
1.10Hz
(DC)
1.00eV
$\sigma(\Omega m)^{-1}$
$1000/T\ ^{o}K^{-1}$
-4
-5
-6
-7
-8
-9
-10
-11
1.2
1.4
1.6
1.8
2.0
2.2
2.4
2.6
2.8
3.0
3.2
3.4

Fig. 2

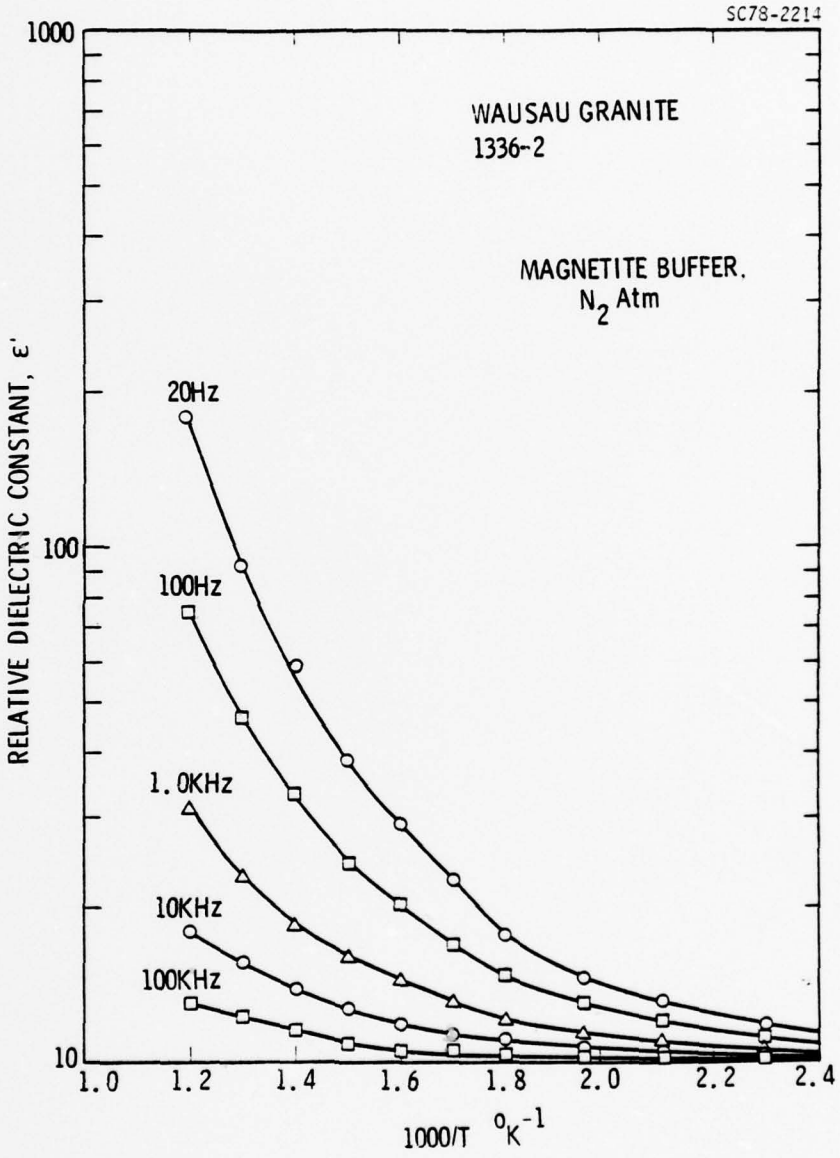
SC78-2214
WAUSAU GRANITE
1336-2
MAGNETITE BUFFER,
N_2 Atm
20Hz
100Hz
1.0KHz
10KHz
100KHz
RELATIVE DIELECTRIC CONSTANT, ε'
1000
100
10
1.0
1.2
1.4
1.6
1.8
2.0
2.2
2.4
1000/T $^{o}K^{-1}$

Fig. 3

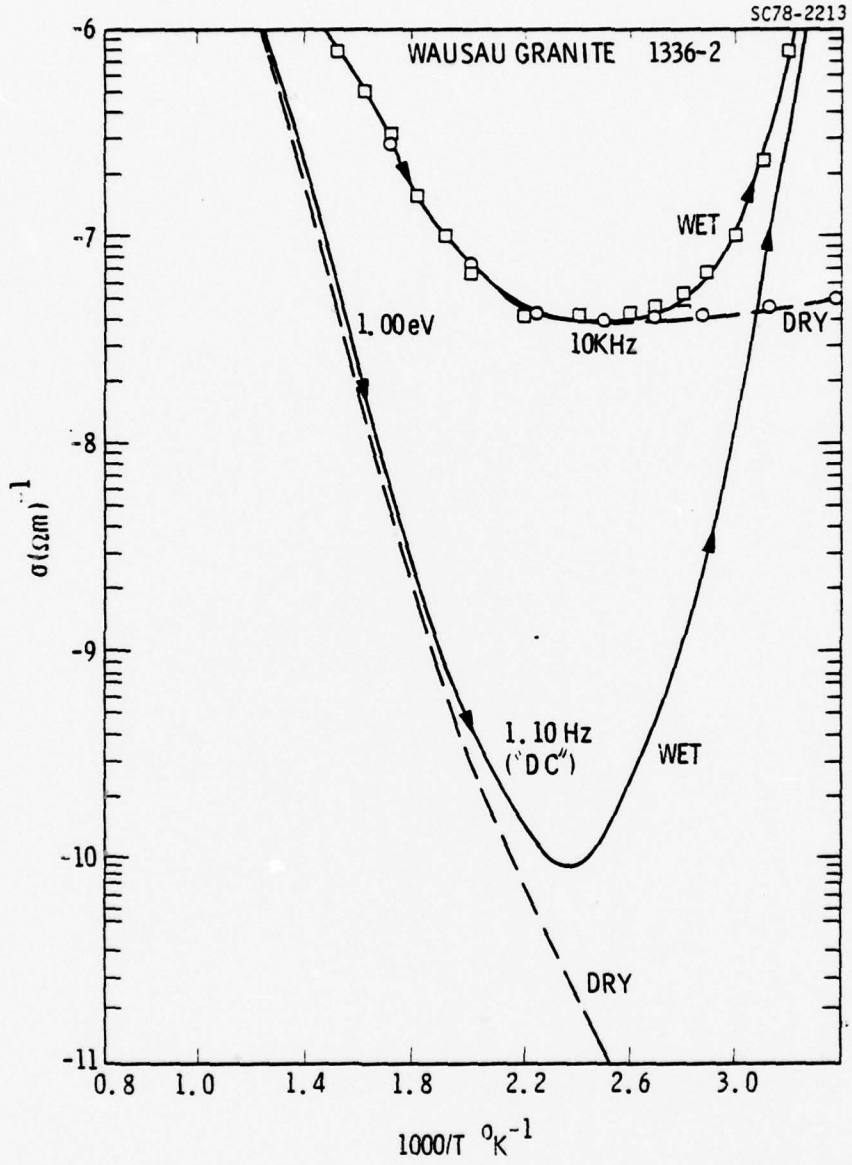
SC78-2213
WAUSAU GRANITE 1336-2
WET
DRY
1.00eV
10KHz
1.10 Hz
("DC")
WET
DRY
-6
-7
-8
-9
-10
-11
σ(Ωm)^-1
0.8
1.0
1.4
1.8
2.2
2.6
3.0
1000/T °K^-1

Fig. 4

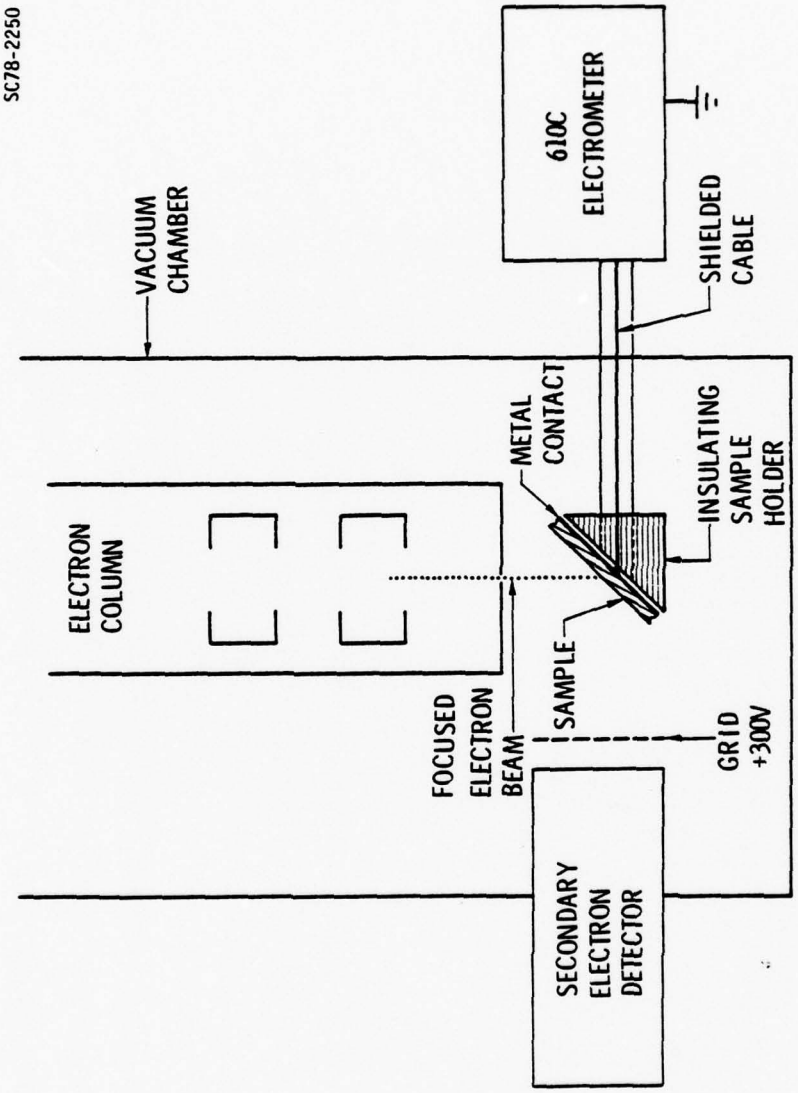
SC78-2250
VACUUM CHAMBER
610C ELECTROMETER
SHIELDED CABLE
METAL CONTACT
INSULATING SAMPLE HOLDER
ELECTRON COLUMN
SAMPLE
FOCUSED ELECTRON BEAM
GRID +300V
SECONDARY ELECTRON DETECTOR

Fig. 5

(a)

(b)

(c)

(d)

Fig. 6

APPENDIX 1

ELECTRICAL PROPERTIES OF FORSTERITE, Mg_2SiO_4 (II)

Submitted for publication to PHYSICAL REVIEW

Rockwell International
Science Center

ELECTRICAL PROPERTIES OF FORSTERITE, Mg_2SiO_4 (II) †

F. J. Morin, J. R. Oliver, and R. M. Housley
Rockwell International Science Center
Thousand Oaks, California 91360

ABSTRACT

In this paper we develop a model for ionic transport in forsterite which predicts a different directional dependence of transport for magnesium interstitials and vacancies. This model, together with dc transport measurements on forsterite into which iron was diffused, suggests that we are dealing with interstitial transport in synthetic forsterite whereas diffusion experiments on olivine reported in the literature have been dealing with vacancy transport. Our transport measurements also support the idea that Fe^{3+} acts as an acceptor level lying 3.0 eV above the valence band of forsterite. Transport measurements are also reported for forsterite into which hydrogen has been diffused.

1.0 INTRODUCTION

In the previous paper[1] we described the dc conductivity of synthetic single crystal forsterite, Mg_2SiO_4. We showed that, at lower temperature, transport was ionic in the (a) and (c) directions and electronic in the (b) direction and, at higher temperature, became dominated by electronic transport in all directions. It was found that, at lower temperature, the directional dependence of ionic conductivity was: $\sigma(a) > \sigma(c) > \sigma(b)$. It was pointed out that this result disagrees with the directional dependence of ionic conductivity found by a number of diffusion experiments performed on olivine,[2-4] namely $\sigma(c) >> \sigma(a) > \sigma(b)$. At the time of writing the previous paper we were thinking in terms of transport by magnesium vacancies. Therefore, the results were analyzed in these terms. In this paper we develop a transport model which suggests that the former order of conductivity is appropriate for magnesium interstitial transport while the latter order of conductivity is appropriate for magnesium vacancy transport. This result requires a change in the nomenclature used in the previous paper but does not change the analysis or the numerical results.

In the previous paper it was suggested that the electronic transport was due to holes in the valence band and an acceptor level located 3.0 eV above the valence band and probably associated with octahedral Fe^{3+}. In this paper we report dc conductivity measurements made on samples into which iron has been diffused. The results of these measurements tend to confirm the idea that ionic transport in forsterite is due to interstitials and that iron acts as an acceptor level.

We also report dc measurements made on samples which have been equilibrated in a hydrogen-containing reducing atmosphere. An attempt is made to understand these results in terms of the ionic transport model.

2.0 IONIC TRANSPORT MODEL

A model for octahedral ion transport is developed in this section based upon a tentative ordering of the octahedral site preference energies, E_s, and the octahedral ion transport energies, E_t, which are required for ions to move between adjacent octahedral sites.

There are four nonequivalent octahedral sites. These sites are designated M1, M2, M3, and M4, and are shown in Fig. 1. They may be described in terms of how they share oxygen with adjacent octahedra which contain magnesium or with adjacent tetrahedra which contain silicon. That is:

M2 shares 1 edge with tetrahedra and 2 edges with octahedra

M1 shares 2 edges with tetrahedra and 4 edges with octahedra

M3 shares 1 face with tetrahedra, 2 faces with octahedra, and 4 edges with octahedra

M4 shares 2 faces with tetrahedra, 2 faces with octahedra, and 2 edges with octahedra

If we assume that the site preference energy is related inversely to the degree to which a particular site shares its oxygens with sites which contain positive magnesium and silicon ions we can order the site preference energies

$$E_s(M2) > E_s(M1) > E_s(M3) > E_s(M4)$$

This ordering is consistent with the fact that M2 and M1 are normally occupied, and M3 and M4 are normally empty. Alternatively, the same ordering for E_s can be obtained by summing the ratios zr^{-1}, where z is the number of unit charges on an ion and r is the distance to the ion for the first shell of neighboring magnesium and silicon ions about a given octahedral site.

Typical situations which follow from this result are shown in Fig. 2. At lower temperature and with no impurities or other lattice defects present, sites M3 and M4 are normally empty. Frenkel pairs might form at higher temperature as site M3 become occupied with the formation of vacancies, V_{M1}, and interstitials, I_{M3}. At still higher temperature V_{M2} and I_{M4} might be produced. When an impurity such as Fe^{3+} substitutes for Mg^{2+}, extrinsic V_{M1} are produced at lower temperature and, possibly, V_{M2} at higher temperature. When an impurity such as Al^{3+} substitutes for Si^{4+} extrinsic I_{M3} are produced at lower temperature and, possibly, I_{M4} at higher temperature.

Ions can move among the octahedral sites by displacement through shared edges, e, or through shared faces, f. The relative energies required for these displacements may be ordered by noting how freely the displaced oxygen ions can move. That is, whether displacement requires oxygen ions to move toward silicon or magnesium or requires the opening of the tetrahedral angle between oxygen-silicon bonds. Table I was constructed with these ideas in mind. From that table we tentatively order the displacement energies as follows:

$$E_t(e1) = E_t(e2)$$

$$E_t(e6) > E_t(e1) > E_t(e4) > E_t(e5) > E_t(e3)$$

$$E_t(f1) = E_t(f3) > E_t(f2)$$

Extrinsic vacancy transport appears to require the least energy in the (c) direction because there are continuous chains of occupied octahedra. There are two possible paths. The first path is the motion of V_{Mg} between M1 sites,

$$(M1 + V_{M1}) \rightarrow (V_{M1} + M1)$$

and the energy required for motion is $E_t(e1)$. The second path alternates between M1 and M2 sites,

$$(V_{M1} + M2 + M1) \rightarrow (M1 + V_{M2} + M1) \rightarrow (M1 + M2 + V_{M1})$$

and requires as the energy for transport some combination of level transport and site preference energies such as:

$$E_t = E_t(e2) + [E_s(M2) - E_s(M1)]_V$$

where the difference in site preference energy is assumed to be reduced by the presence of the vacancy as indicated by the subscript V. The first path apears to require the lesser energy.

There are no continuous chains of occupied octahedra in the (a) and (b) directions and, therefore, the relatively low-energy vacancy transport found in the (c) direction is impossible and transport must depend upon the thermal generation of an adjacent interstitial. The low probability of this event may be influenced somewhat by the presence of the vacancy located two octahedra removed from the ion which must move into interstitial position for the vacancy transport to occur. In the (a) direction this process yields the displacement

$$(M1 + M4 + V_{M1}) \rightarrow (V_{M1} + I_{M4} + V_{M1}) \rightarrow (V_{M1} + M4 + M1)$$

which probably requires an energy of the form

$$E_t = E_t(f1) + [E_s(M4) + E_s(M1)]_V$$

Vacancy transport in the (b) direction requires the production of an interstitial plus the creation of V_{M2}. From these considerations we conclude concerning the anisotropy of transport by extrinsic vacancies:

$$\sigma(c) >> \sigma(a) > \sigma(b)$$

Extrinsic transport by interstitials appears to involve a cooperative process. There are no continuous chains of unoccupied octahedra in any direction. Therefore, an ion must move out of a normally occupied site in order that an interstitial may move in. In this way an interstitial moves to the next nearest octahedron. If the vacancy concentration involved were the normal equilibrium concentration, extrinsic interstitial transport would be a very low level process. However, it seems likely that interstitials can move by means of a nonequilibrium, cooperative process. *Thus we have for extrinsic* interstitial transport in the (a) direction the displacement

$$(I_{M3} + M2 + M3) \rightarrow (I_{M3} + V_{M2} + I_{M3}) \rightarrow (M3 + M2 + I_{M3})$$

or, more simply

$$(I_{M3} + M2 + M3) \rightarrow (M3 + M2 + I_{M3})$$

by the coordinated motion of I_{M3} and M2. These displacements are written to denote three octahedra which share faces in the (a) direction. The first site, normally unoccupied M3, is occupied by an interstitial magnesium I_{M3}. The second site is a normally occupied M2 site and the third a normally unoccupied M3 site. The energy for the displacement is

$E_t = E_t(f2) + [E_s(M2) - E_s(M3)]_I$ where the site preference energy

difference is much reduced by the presence of the interstitial so that the cooperative displacement can occur easily. A similar displacement is possible in the (c) direction. However, in the (c) direction the effect of the interstial upon the difference in site preference energies is significantly less because the magnesium ions are much further apart in a line of octahedra which share edges than they are in the (a) direction where the line of octahedra share faces. Interstitial transport in the (b) direction requires the formation of I_{M4} which appears to be an event of lower probability. Thus we conclude that for extrinsic interstitials the anisotropy of transport is

$$\sigma(a) > \sigma(c) > \sigma(b)$$

The model suggests that we are dealing with extrinsic interstitials in synthetic forsterite while the diffusion experiments reported in the literature and involving olivine are dealing with extrinsic vacancies. Since extrinsic vacancies occur to charge compensate Fe^{3+} iron, it is reasonable to assume that they exist in large concentrations in olivine. The presence of extrinsic interstitials in forsterite suggests the possibility that the dominant impurity in our samples is Al^{3+} substituting for silicon. With these ideas in mind the experiments described in the next section were performed to compensate Al^{3+} with Fe^{3+} and thus to reduce the concentration of interstitials or to produce a condition for extrinsic vacancy transport.

3.0 IRON DIFFUSION EXPERIMENTS

High purity iron was sputtered onto oriented samples of forsterite from boul F2 and diffused at 1500K in oxygen for 100 hr. Contact preparation and the sample holder have been described in the previous paper. The samples were equilibrated at the highest temperature of measurement for 2 hr in oxygen and then measured with both heating and cooling in oxygen. The measurements were reproducible.

The dc conductivity, following iron diffusion, is shown in Fig. 3 for the three orientations and compared with the (b) direction conductivity prior to iron diffusion. The curves show a lower temperature region which is assumed to be due to ionic transport and a higher temperature region which has about the same slope as the (b) direction prior to iron diffusion and, therefore, is assumed to be due to electronic transport. If we compare these curves with those obtained prior to the introduction of iron (Fig. 8 of the previous paper), we note that introduction of iron has reduced ionic transport, increased electronic transport and caused a curvature which was not evident before in the higher temperature part of the electronic transport. The mobile hole concentration may be estimated by subtracting the ionic from the electronic conductivity and dividing the remainder by the product of electronic charge and an assumed hole mobility, $q\mu_p = 1.6 \times 10^{-23}$ cm^2 V^{-1} sec^{-1}. Hole concentrations so obtained are shown in Fig. 4. Using conventional methods[5] and assuming hole mass equal to rest mass, we have calculated a fit to these data. The parameters

determined by this calculation are shown in Table II. The curvature in the hole concentration curves allows an independent estimate of acceptor and donor concentrations N_A and N_D. While this was not possible for the sample prior to iron diffusion because the results were a straight line, we could determine the ratio $(N_A - N_D)\ N_D^{-1}$. If we assume that the donor concentration remained fixed at $N_D \sim 10^{19}\ m^{-3}$ during iron diffusion, then the acceptor concentration prior to iron diffusion was determined from that ratio to be $N_A = 3.5 \times 10^{20}\ m^{-3}$. These quantities are shown in () in Table II. They indicate that iron diffusion has increased the acceptor concentration by a factor of 100.

The ionic tail on curve (c) Fig. 3 shows a slope $E_t = 1.33$ eV, which is characteristic of mobile ion transport in the (c) direction. This indicates that all of the ions are mobile, and hence that we may calculate the mobile ion concentration using Eq. (2) of the previous paper. We find the mobile ion concentration to be $3.6 \times 10^{21}\ m^{-3}$ after the introduction of iron as compared to $3.5 \times 10^{23}\ m^{-3}$ originally. Total mobile ion concentration has been reduced by a factor of 100 by iron diffusion. The ionic tails on curves (a) and (b) of Fig. 3 show slopes which are greater than the transport energies which indicate that some of the ions are bound. Therefore, these tails cannot be analyzed easily to yield total mobile ion concentration. However, the results suggest strongly that the introduction of iron has decreased the mobile ion concentration by more than an order of magnitude in these samples.

It is to be noted that the amount of Fe^{3+} introduced by diffusion as determined by the change in acceptor concentration, N_A, is $\sim 10^{22}$ m^{-3} while the amount determined from the decrease in mobile interstitials, N_I, is $\sim 10^{23}$ m^{-3}. It is believed that this discrepancy is a result of our choice of ionic and electronic mobilities. Recall that in the previous paper the preexponential factor determined by fitting the mobile ion concentration curves was 1800 times the known density of states. This factor, e^{α}, is assumed to include the temperature coefficients of E_t and of E_b. Thus if we increase the preexponential factor in the mobility expression by a factor of ten to account for the temperature coefficient of E_t, the value determined for N_I will be decreased by a factor of ten and the discrepancy will disappear.

A neutral molecule of forsterite which contains Fe^{3+} iron and charge compensating magnesium vacancies can be written:

$$(Mg_2^{2+}\ Fe_2^{3+}\ V_{Mg}^{2-})\ Si_2^{4+}\ O_8^{2-} \qquad (1)$$

A neutral molecule containing Al^{3+} in place of silicon and with charge compensating interstitials can be written:

$$(Mg_8^{2+}\ I_{Mg}^{2+})\ (Al_2^{3+}\ Si_2^{4+})\ O_{16}^{2-} \qquad (2)$$

A neutral molecule in which iron and aluminum compensate each other can be written:

$$(Mg_3^{2+}\ Fe^{3+})\ (Al^{3+}\ Si^{4+})\ O_8^{2-} \qquad (3)$$

We assume that our situation may be represented by (2) + (3). That is, the concentration of Al^{3+} exceeds the concentration of Fe^{3+} in the samples prior to the introduction of iron. Following the introduction of iron, the situation is approximately described by (3). Forsterite in the state represented by (3) would be expected to display only electronic transport in all directions over our temperature range of measurement.

A simplified energy level diagram which describes the situation before and after the introduction of iron is shown in Fig. 5. In Fig. 5(a), $[Al^{3+}] > [Fe^{3+}]$ and we have high-lying I_{Mg} donors which are empty, empty Fe^{3+} acceptors lying near mid gap and low-lying Al^{3+} acceptors which are full. In Fig. 4(b) the introduction of additional iron has compensated the aluminum so that $[Fe^{3+}] = [Al^{3+}]$. I_{Mg} donors have been eliminated and Fe^{3+} acceptor concentration has increased. In Fig. 5(c) $[Fe^{3+}] > [Al^{3+}]$ and compensating V_{Mg} have been introduced which produce low-lying V_{Mg} acceptor levels which are full. We had hoped to achieve condition (c) with the diffusion experiments and study vacancy transport but apparently failed to go beyond condition (b).

The iron diffusion experiments support the ideas that we are dealing with extrinsic I_{Mg} transport and that Fe^{3+} acts as an acceptor lying 3.0 eV above the valence band.

4.0 HYDROGEN DIFFUSION EXPERIMENTS

In order to investigate the effect of a hydrogen-containing reducing atmosphere on forsterite, a set of oriented samples from boul F2 were

equilibrated at 1350K and measured in nitrogen which contained 4% hydrogen. We assume that oxygen is not mobile at the temperatures of the experiment and that hydrogen diffuses into the forsterite. It is not unusual for hydrogen to diffuse into oxides:[6,7] the proton moves from oxygen to oxygen in the form of OH^- and may become trapped at an oxygen which is adjacent to an aliovalent ion with a net negative charge; the electron, which accompanies the proton, falls into an empty acceptor level. The hydrogen solubility depends upon the concentration of acceptor levels and upon the electronic equilibria.

The dc conductivity following hydrogen treatment is compared with prior measurements made in oxygen and shown in Figs. 6, 7, and 8. Using the procedures described in the previous paper, electronic and ionic components of conductivity were separated and mobile ion concentrations were determined. The mobile ion concentrations are shown in Figs. 9, 10, and 11 and the parameters determined by calculating a fit to these data are shown in Table III. In addition to these results, a search for the O-H stretching frequency was made in the range 3300 cm^{-1} to 3700 cm^{-1} with a sensitivity of $\sim 10^{22}$ m^{-3} protons. No protons were detected. Also, the EPR signal of Fe^{3+} was observed before and after hydrogen treatment. The signal was significantly decreased by the hydrogen treatment.

Transport measurements indicate that the parameters E_t, E_b, and $e N_L$ remain essentially the same with hydrogen treatment but that both the total concentration of mobile ions, N_I, and of binding centers, N_M, have increased and by about the same amount in a given sample. These results suggest the increased transport is not due to mobile protons but to an increase in the total concentration of mobile interstitials. Furthermore,

mobile proton transport would be expected to be isotropic because the oxygen lattice is nearly isotropic while the observed transport is anisotropic. If we use the ionic mobility suggested in the previous section which is a factor of ten greater than that used to obtain the results in Figs. 9, 10, and 11 and in Table III, we infer that roughly 10^{22} m^{-3} hydrogens were dissolved in the forsterite samples. The decrease in the EPR signal of Fe^{3+} also suggests that protons diffused into the samples and that the electrons brought with the protons converted Fe^{3+} acceptors to Fe^{2+}.

Let us assume that in our experiment the negative aliovalent site is tetrahedral Al^{3+} and that the empty acceptor level is octahedral Fe^{3+}. If, prior to hydrogen treatment, the negative Al^{3+} site is neutralized by a positive octahedral Fe^{3+}, the most likely location for the Fe^{3+} would be the M3 site. This site shares a face with a tetrahedron and takes full advantage of the coulomb attraction between the two aliovalent ions. Now the addition of hydrogen converts the Fe^{3+} to I_{Fe}^{2+} which is similar to interstitial magnesium. This also releases the adjacent Al^{3+} to act as a normal binding site for mobile interstitials. In this way both N_I and N_M increase by the same amount as was observed. However, this model does not account for the location of the proton.

An alternative model is one in which the Fe^{3+} occupies a substitutional M1 or M2 site and some of the interstitial magnesium are strongly bound to an aliovalent ion site which has a net charge of 2-. The addition of hydrogen converts the iron to substitutional Fe^{2+} and the proton converts the charge on the aliovalent ion site to 1-. This reduces the

binding energy of the site to that of a singly charged site and thus both N_I and N_M increase together.

Clearly, neither of these models is complete and more work is required in order to understand the role of hydrogen in forsterite.

REFERENCES

† Work partially supported by ONR Contract No. N00014-76-C-0653.

1. F. J. Morin, J. R. Oliver, and R. M. Housley, Phys. Rev. B, 16, 4434 (1977)
2. D. K. Buening and P. R. Buseck, J. Geophys. Res., 78, 6852 (1973)
3. A. M. Clark and J. V. P. Long, "International Thomas Graham Memorial Symposium", 1969, edited by J. N. Sherwood et al (Gordon and Breach, New York, 1970)
4. D. J. Misener, "Geochemical Transport and Kinetics", Publication 634 (Carnegie Institute, Washington, D. C., 1973), p. 117
5. "Semiconductors", edited by N. B. Hannay (Reinhold Publishing Corporation, New York, 1959)
6. R. G. Smith, D. B. Fraser, R. T. Denton and T. C. Rich, J. Appl. Phys., 39, 4600 (1968)
7. S. Singh, H. J. Levinstein, and L. G. von Uitert, Appl. Phys. Lett., 16, 176 (1970)

FIGURE CAPTIONS

Figure 1 Forsterite structure showing the four nonequivalent octahedral sites M1, M2, M3, and M4. Large spheres, oxygen; intermediate spheres, magnesium; small spheres, silicon.

Figure 2 Diagram of site preference energy and site occupancy for four situations: (a) no defects present, (b) Frenkel defects, (c) extrinsic vacancy, (d) extrinsic interstitial.

Figure 3 Measured electrical conductivity of forsterite for the three crystallographic directions (a), (b), and (c) following iron diffusion. The lowest curve is for the (b) direction prior to iron diffusion.

Figure 4 Estimated hole concentration of forsterite for crystallographic directions (a), (b), and (c) following iron diffusion. The lowest curve is for the (b) direction prior to iron diffusion. The points were determined from measured conductivity and an assumed mobility of $\mu_h = 10^{-4}\ m^2\ V^{-1}\ sec^{-1}$. The curves were calculated using conventional statistics.

Figure 5 Schematic energy level diagrams showing the band gap of forsterite containing donor levels for interstitial magnesium, I_{Mg}, acceptor levels for octahedral Fe^{3+}, acceptor levels for tetrahedral Al^{3+}, and acceptor levels for magnesium vacancies, V_{Mg}, for three cases of relative Fe^{3+} and Al^{3+} concentration.

Figure 6 Measured electrical conductivity for the (a) direction of forsterite equilibrated in oxygen and in hydrogen. The dashed line represents the electronic component of the conductivity in oxygen.

Figure 7 Measured electrical conductivity for the (b) direction of forsterite equilibrated in oxygen and in hydrogen.

Figure 8 Measured electrical conductivity for the (c) direction of forsterite equilibrated in oxygen and in hydrogen. The dashed line represents the electronic component of the conductivity in oxygen.

Figure 9 Mobile interstital concentration for the (a) direction of forsterite equilibrated in oxygen and in hydrogen. The points were determined from conductivity measurements and the solid lines were calculated. The dashed curves are the two components required to calculate the fit to curve (H_2).

Figure 10 Mobile interstitial concentration for the (b) direction of forsterite equilibrated in hydrogen. The points were determined from conductivity measurements and the solid line was calculated.

Figure 11 Mobile interstitial concentration for the (c) direction of forsterite equilibrated in oxygen and in hydrogen. The points were determined from conductivity measurements and the solid lines were calculated.

TABLE CAPTIONS

Table I Path designation and oxygen ion motion required for movement of magnesium ions among the M1, M2, M3 and M4 octahedral sites. Movement, e, is through a shared octahedral edge and movement, f, is through a shared octahedral face.

Table II Parameters determined from an analysis of the hole concentration results of Figure 4.

Table III Parameters determined from an analysis of the mobile interstitial concentration shown in Figures 9, 10, and 11.

TABLE I

Displacement		Path	Oxygen ion Motion
M1	M1	e1	one toward silicon, one toward magnesium
M1	M2	e2	one toward silicon, one toward magnesium
M1	M3	e3	no direct motion toward other ions
M2	M4	e4	both toward magnesium
M2	M3	e5	one toward magnesium
M3	M4	e6	through edge shared with tetrahedron
M1	M4	f1	opening tetrahedron edge
M2	M3	f2	one toward silicon
M2	M3	f3	opening tetrahedron edge

TABLE II

Sample	N_A (m^{-3})	N_D (m^{-3})	$\frac{N_A - N_D}{N_D}$	E_A (eV)
(a)	2×10^{22}	1×10^{19}	2000	3.05
(b)	2.5×10^{22}	5.7×10^{19}	435	3.05
(b)	(3.5×10^{20})	(10^{19})	34	2.95
(c)	1×10^{22}	1.6×10^{19}	665	3.05

TABLE III

Orientation	(a)		(b)	(c)	
	oxidized	reduced	reduced	oxidized	reduced
E_t (eV)	1.00	1.00	1.33	1.33	1.33
E_b (eV)	2.08	1.95	2.10	2.10	1.80
$e^{\alpha}N_L$ (m^{-3})	5×10^{31}	5×10^{31}	5×10^{31}	5×10^{31}	5×10^{31}
N_I (m^{-3})	6.5×10^{21}	1.0×10^{23}	8×10^{22}	5.5×10^{22}	3×10^{23}
N_M (m^{-3})	6.5×10^{21}	1.7×10^{23}	8×10^{22}	5.42×10^{22}	3×10^{23}

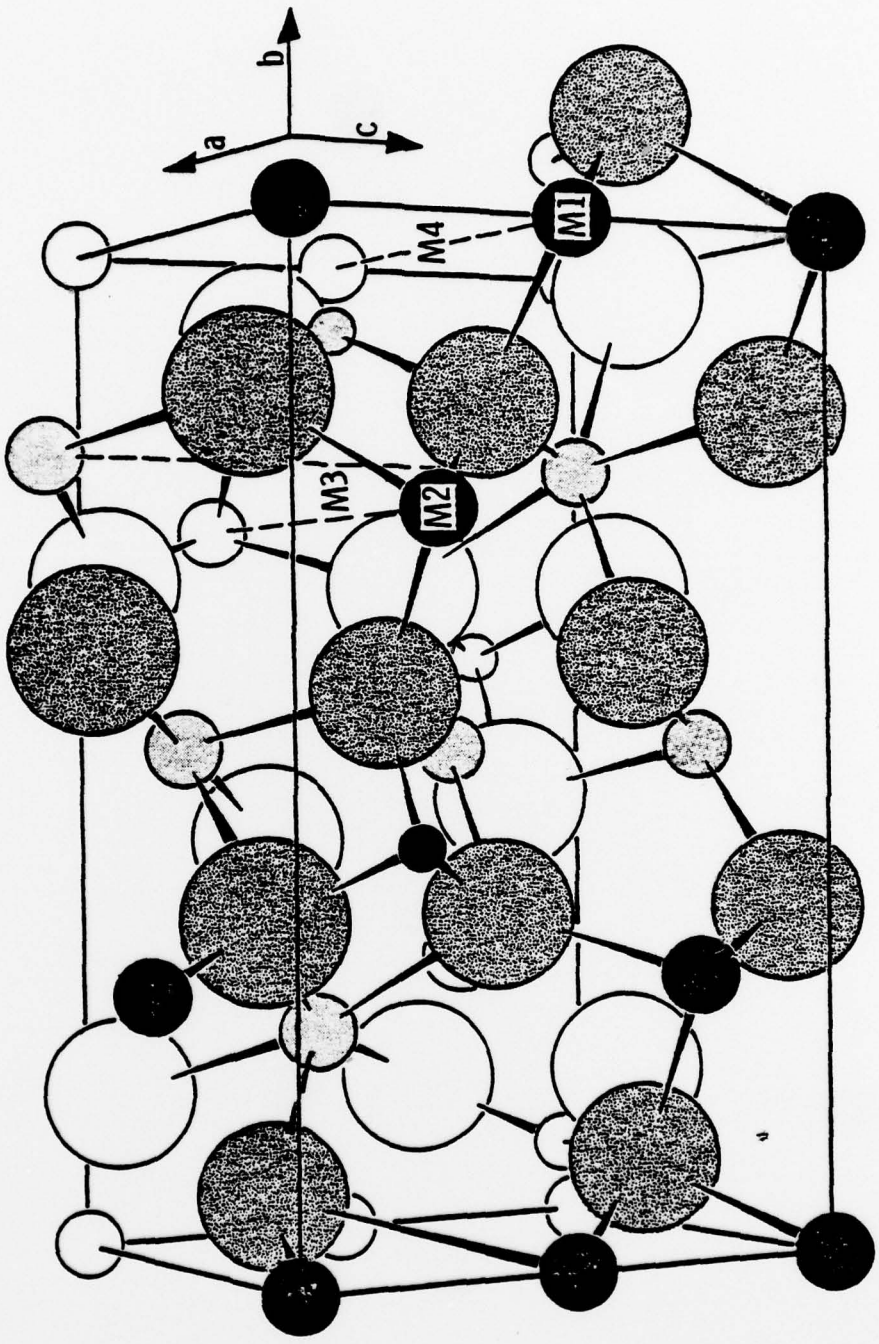

SC78-1062

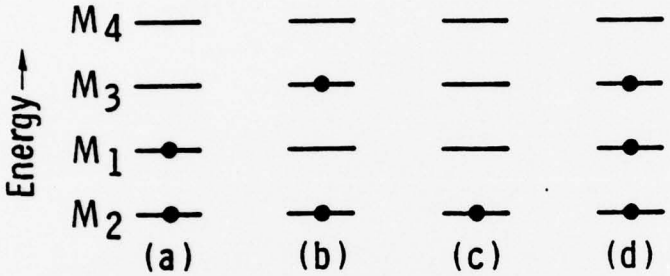
Energy
M4
M3
M1
M2
(a)
(b)
(c)
(d)

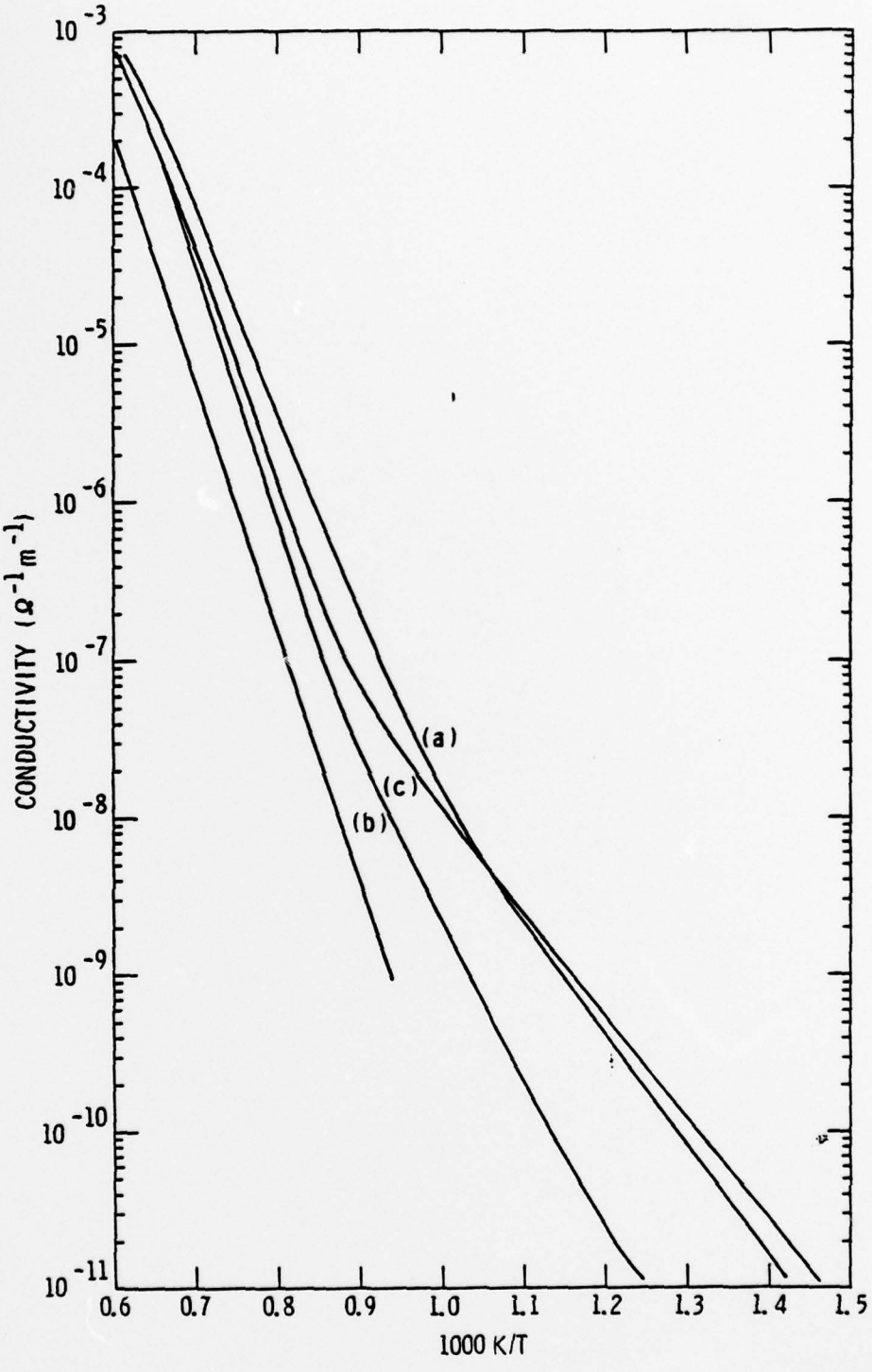
CONDUCTIVITY ($\Omega^{-1}m^{-1}$)
10^{-3}
10^{-4}
10^{-5}
10^{-6}
10^{-7}
10^{-8}
10^{-9}
10^{-10}
10^{-11}
0.6
0.7
0.8
0.9
1.0
1.1
1.2
1.3
1.4
1.5
1000 K/T
(a)
(c)
(b)

SC78-726

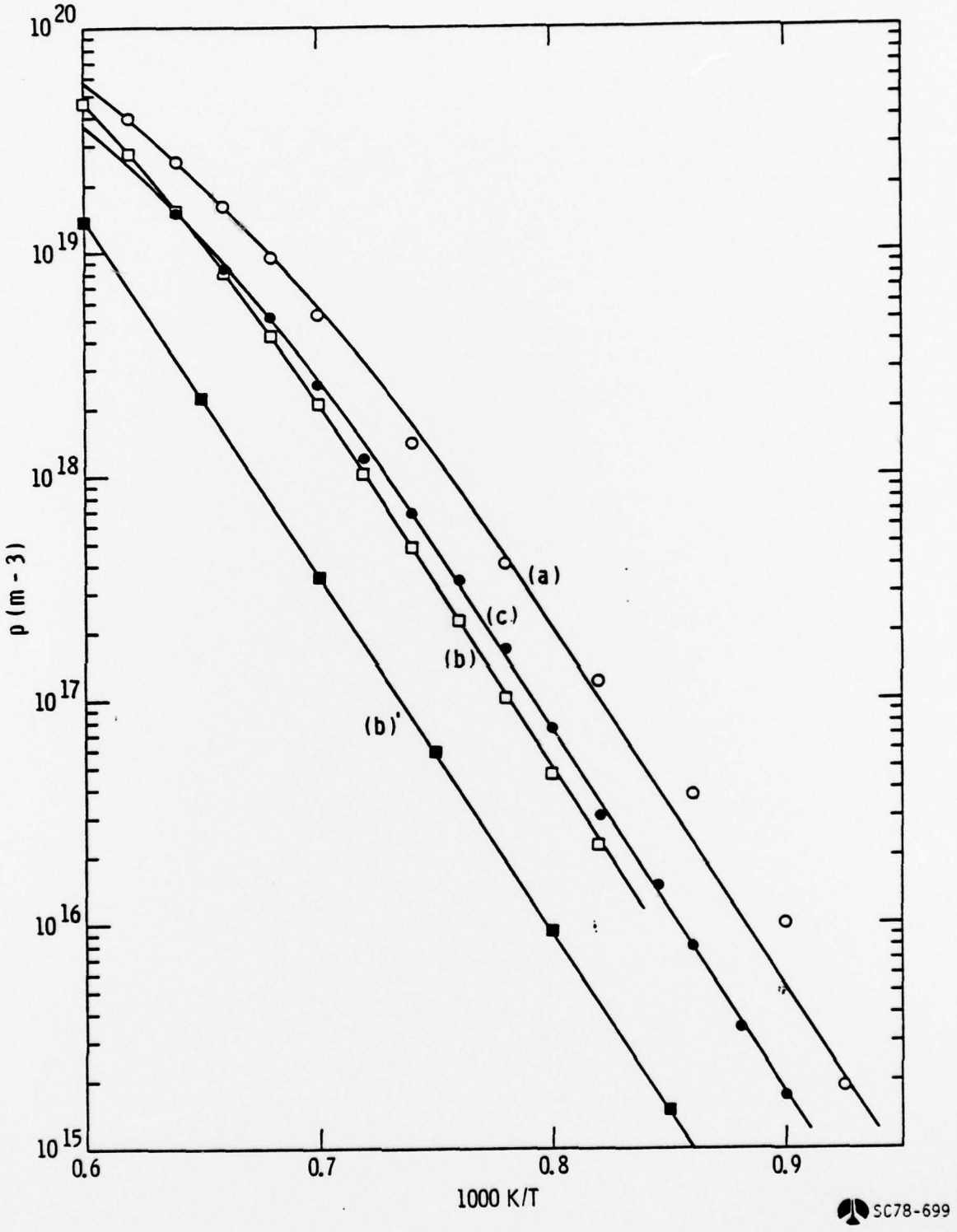
10^{20}
10^{19}
10^{18}
10^{17}
10^{16}
10^{15}
p (m - 3)
0.6
0.7
0.8
0.9
1000 K/T
(a)
(c)
(b)
(b)'
SC78-699

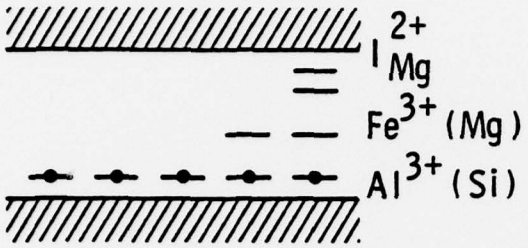

(a)

$[Al^{3+}] > [Fe^{3+}]$

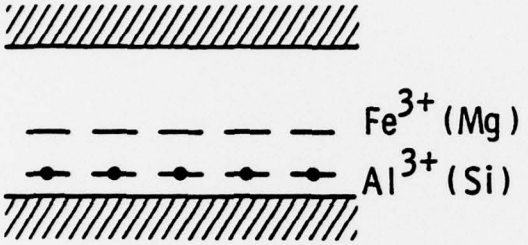

(b)

$[Al^{3+}] = [Fe^{3+}]$

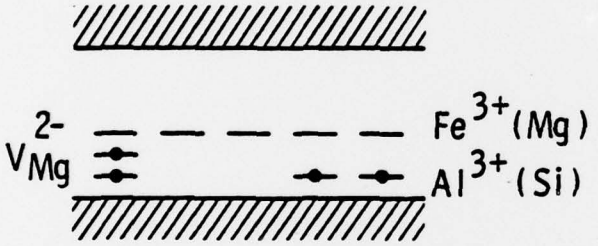

(c)

$[Al^{3+}] < [Fe^{3+}]$

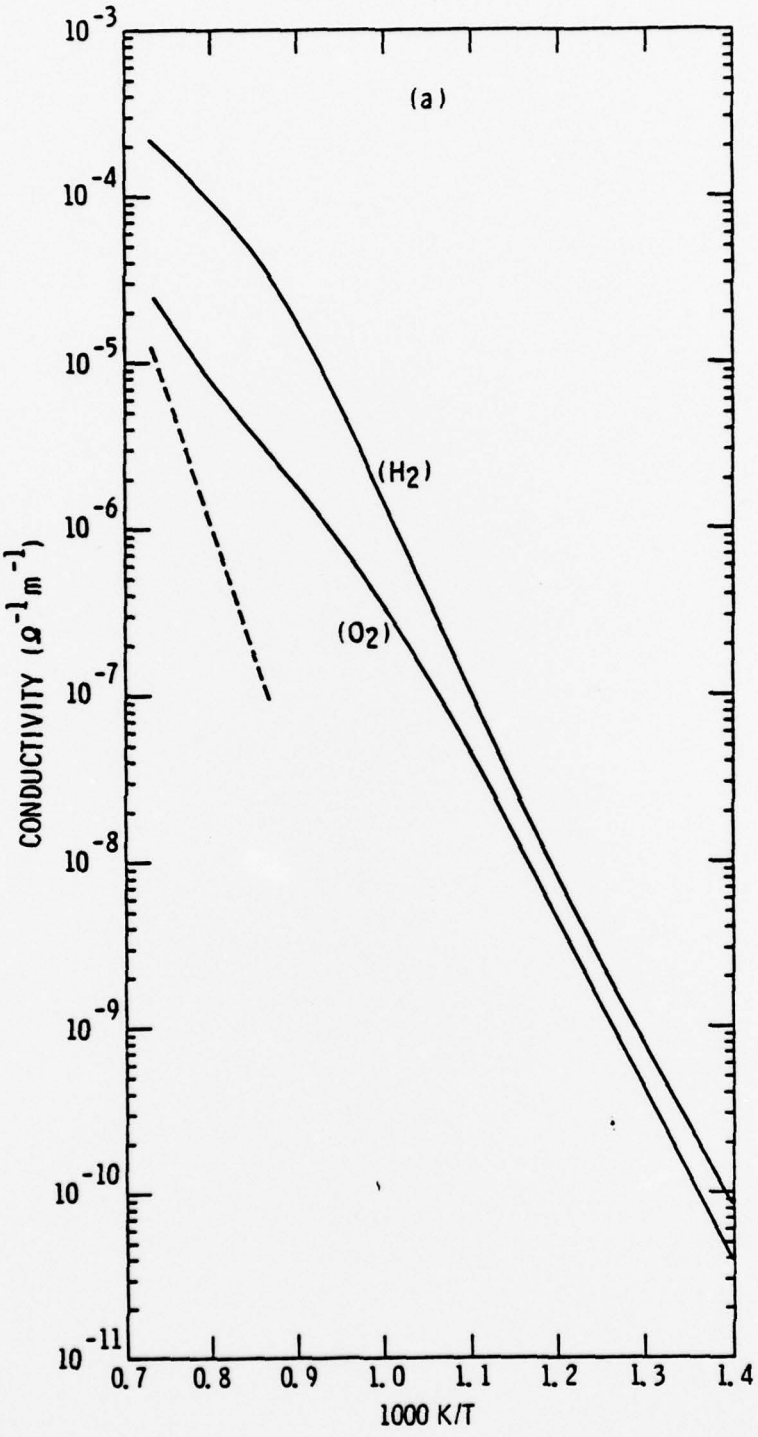
(a)
10^{-3}
10^{-4}
10^{-5}
10^{-6}
10^{-7}
10^{-8}
10^{-9}
10^{-10}
10^{-11}
CONDUCTIVITY ($\Omega^{-1}m^{-1}$)
(H_2)
(O_2)
0.7
0.8
0.9
1.0
1.1
1.2
1.3
1.4
1000 K/T

SC78-727

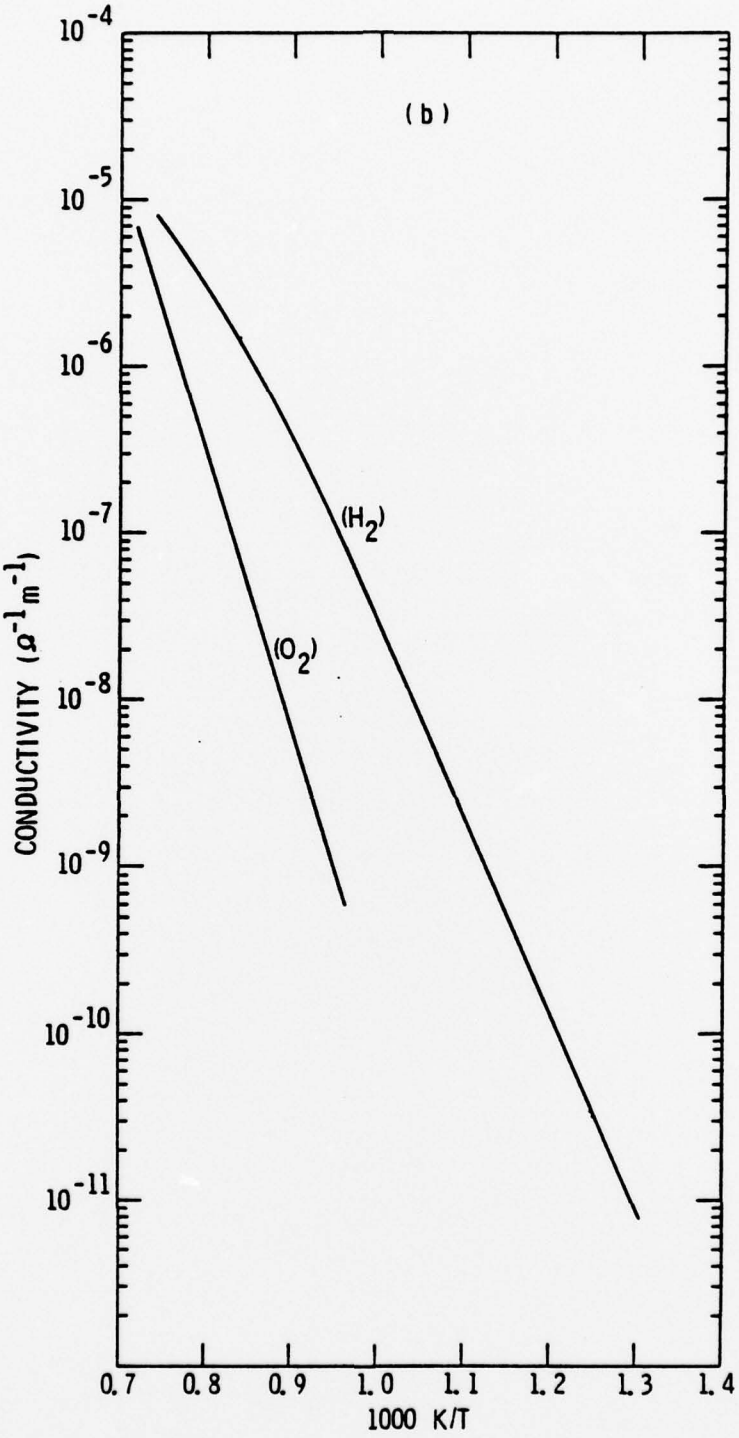
(b)
10^{-4}
10^{-5}
10^{-6}
10^{-7}
10^{-8}
10^{-9}
10^{-10}
10^{-11}
CONDUCTIVITY ($\Omega^{-1}m^{-1}$)
(H_2)
(O_2)
0.7
0.8
0.9
1.0
1.1
1.2
1.3
1.4
1000 K/T

SC78-728

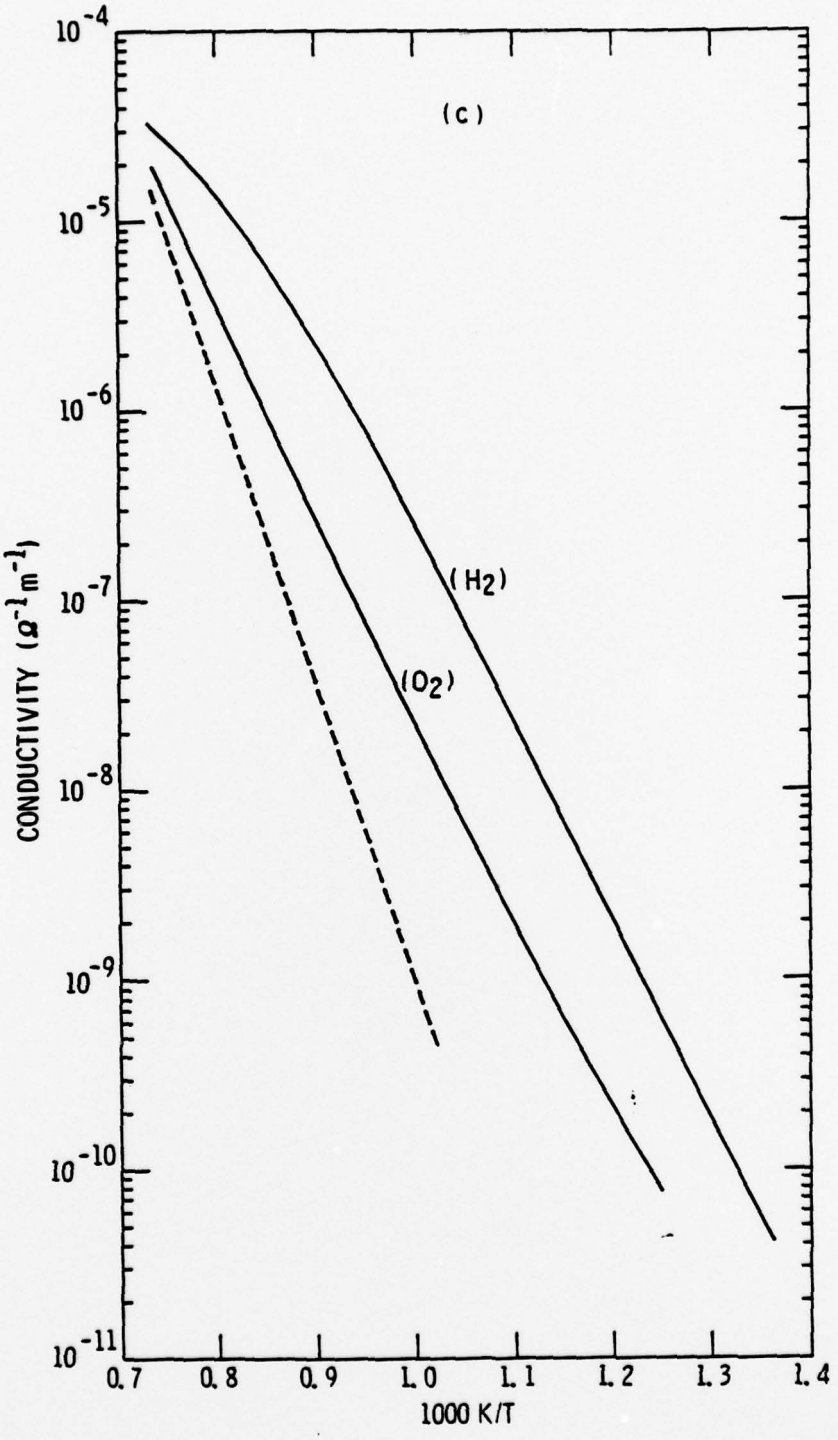
(c)
10^{-4}
10^{-5}
10^{-6}
10^{-7}
10^{-8}
10^{-9}
10^{-10}
10^{-11}
CONDUCTIVITY ($\Omega^{-1}m^{-1}$)
(H_2)
(O_2)
0.7
0.8
0.9
1.0
1.1
1.2
1.3
1.4
1000 K/T

SC78-729

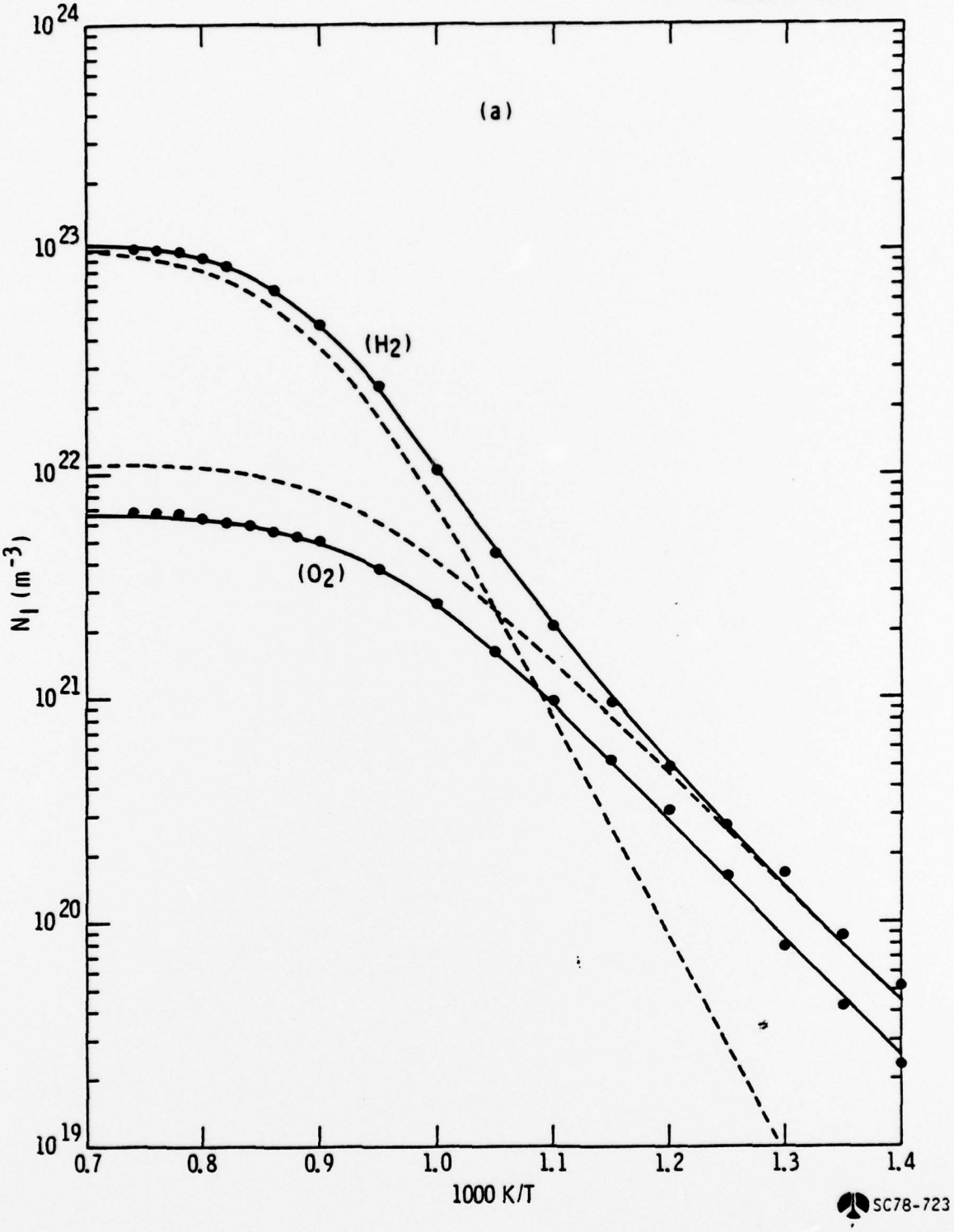
(a)
10^{24}
10^{23}
10^{22}
10^{21}
10^{20}
10^{19}
N_I (m^{-3})
(H_2)
(O_2)
0.7
0.8
0.9
1.0
1.1
1.2
1.3
1.4
1000 K/T
SC78-723

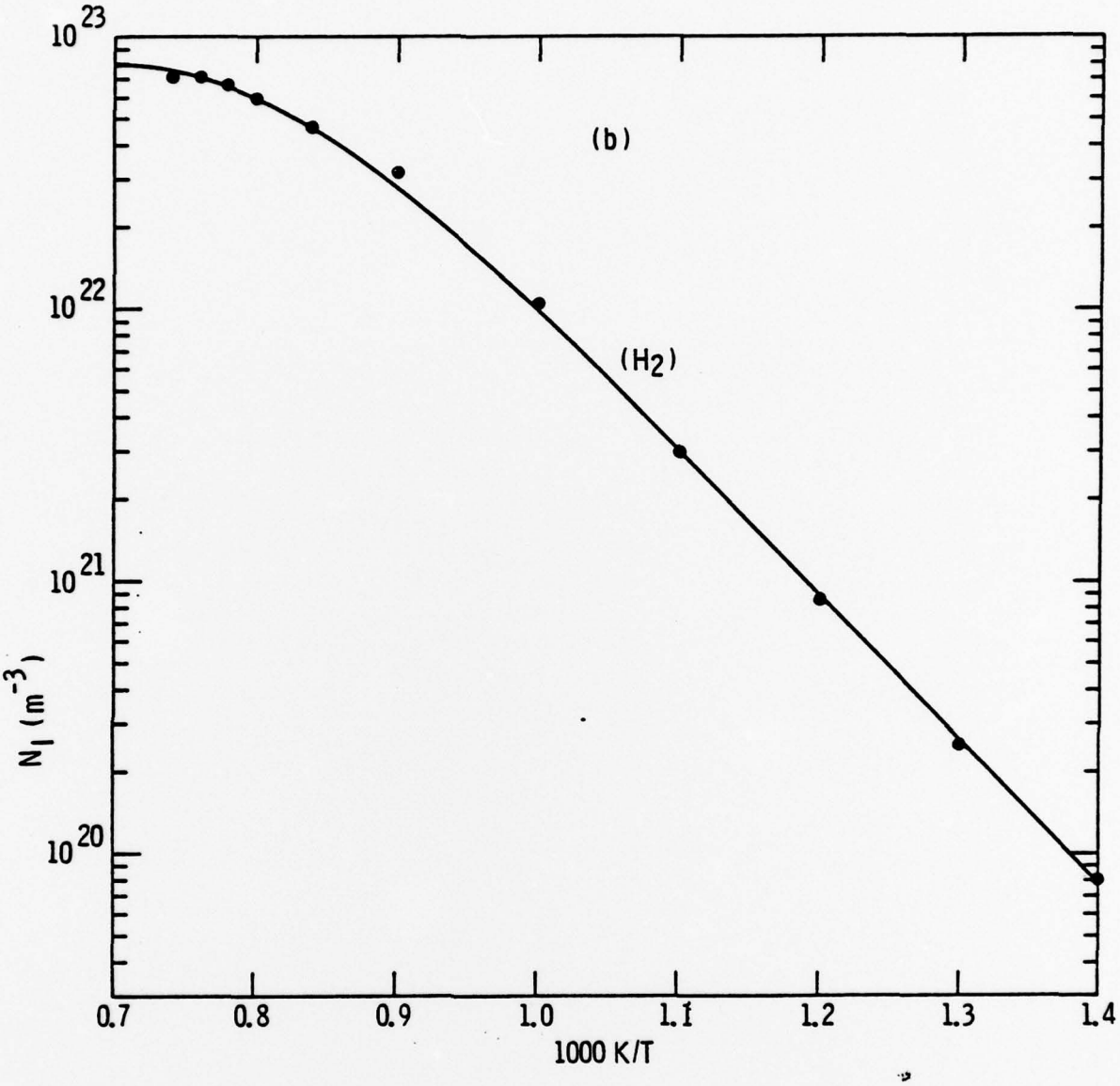
(b)
(H_2)
$N_1\ (m^{-3})$
10^{23}
10^{22}
10^{21}
10^{20}
0.7
0.8
0.9
1.0
1.1
1.2
1.3
1.4
1000 K/T

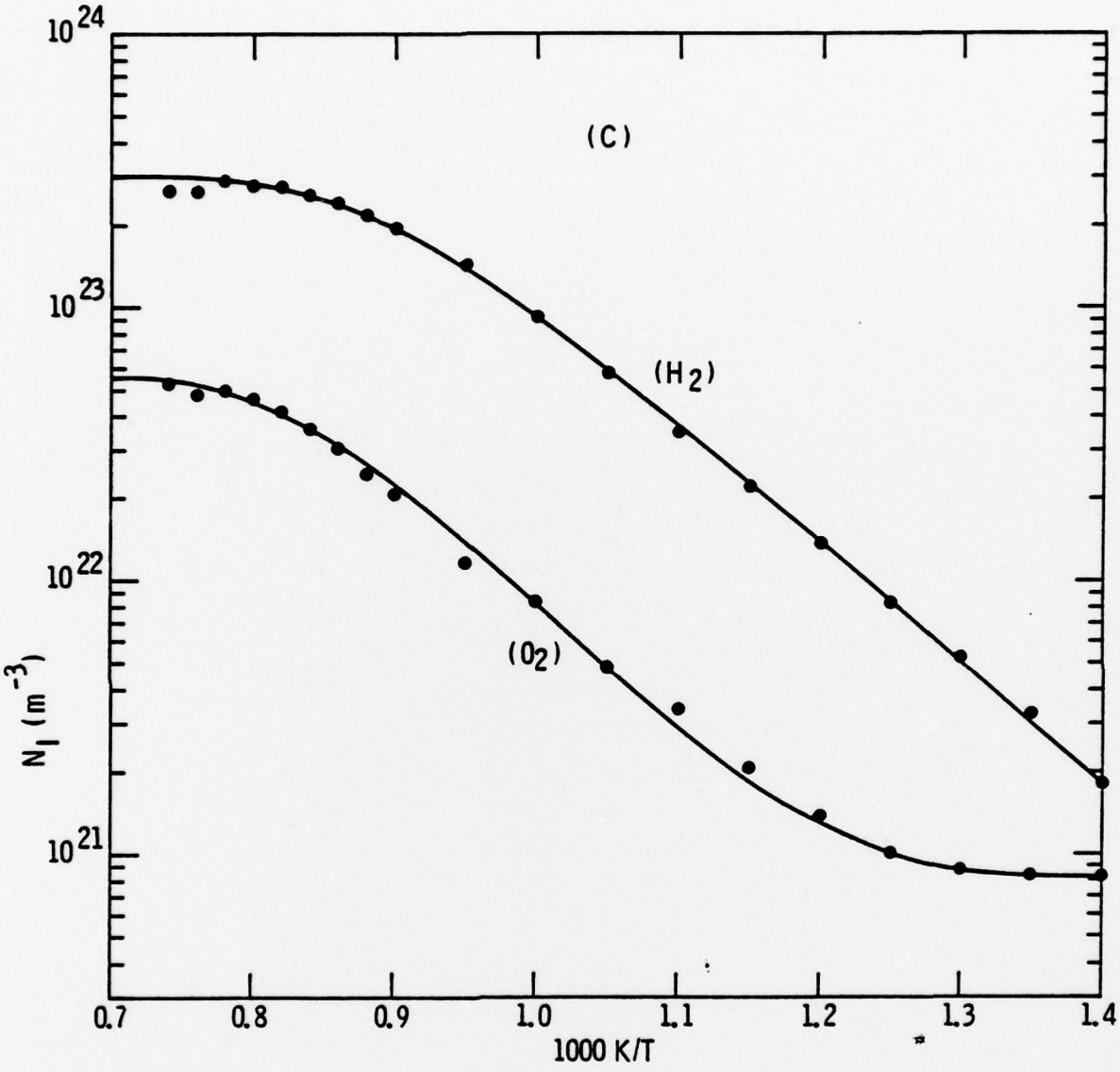

SC78-725